# Solar Physics and Implications to Exotic Particles

*MSc. Project Report*
*Submitted by*

**Eleena Gupta**
(195120026)

Under the Guidance of
**Prof. Vikram Rentala**


**Department of Physics**
**Indian Institute of Technology, Bombay**
**Mumbai-400076**
**2020**

# Abstract

Stellar physics has always been an area of active research. Constructing the stellar models to match the observations offers a unique window into the interior of the stars. Helioseismology, the study of solar oscillations has allowed us to know the Solar structure to high precision. This has allowed us to use the Sun as a laboratory to test the exotic particle physics. The main test of the theory of stellar evolution is the agreement between the stellar model and the helioseismology. But, the new revision of abundances to a lower metallicity value has shown the disagreement between the two and this is referred to as the 'Solar Abundance problem.' Here in this review we describe the theory behind the construction of stellar models and the physics of stellar oscillations. We also discuss the Helioseismic techniques : observations and inversions to obtain details of the stellar structure. We focus on the solar abundances and their consequences on the stellar evolution and also discuss some of the attempts to solve the solar abundance problem. We also discuss the use of helioseismology to put constraints on exotic particles and to probe the dark matter content in the universe.

# Acknowledgements

I would like to express my sincere gratitude towards my supervisor Prof. Vikram Rentala for giving me this opportunity to explore the field of Astro-particle physics. His support, encouragement, patience and enthusiasm towards the work has deeply inspired me. It is a great privilege and honor to work and study under his guidance. I would like to thank my parents and my brother for their love, care and support throughout my life. I wish to extend my special thanks to my friends Saloni, Satvik and Anuj for their help and feedback on the report.

# Contents

# Chapter 1

# Introduction

The Physics of stars and the details of the stellar interior have always been the area of interest of people since ages. Especially the structure of the nearest star Sun has been explored the most. There have been numerous attempts to model the basic structure of a star and hence obtain certain knowledge about them. Arthur Eddington began his book "The Internal Constitution of the Stars" lamenting the fact that the deep interior of the Sun and stars is more inaccessible than the depths of space since we so not have an "appliance" that can ". . . pierce through the outer layers of a star and test the conditions within". Eddington went on to say that perhaps the only way of probing the interiors of the Sun and stars is to use our knowledge of basic physics to determine what the structure of a star should be.

The dominant approach towards stellar physics has been to model the stellar structure using basic equations and compare the results with the observations. One of the tool which can be used to probe the interior is Helioseismology for the Sun or Asteroseismology for other stars. The oscillations on the surface of stars observed are the normal mode oscillations with small amplitudes and can be explained using the basic physics equations and hence can provide details of the interior. They can be expressed in terms of the spherical harmonics as they represent the normal modes on the surface of a sphere. They are classified into $p$-modes, $g$-modes and $f$-modes depending on the main restoring force for the respective oscillation modes. There have been numerous experiments to detect the solar oscillations and hence collect the data using the doppler velocity observations and resolving it to get the normal mode frequencies. This observational data can be inverted to determine the solar properties such as the solar helium abundance , radius of convection zone and also the radial profile of the sound speed and density inside the Sun. and it also reflects upon the rotational profile of the Sun. Other than the helioseismic observations, we can also observe the solar neutrinos as well as measure the elemental abundances of the solar interior using photospheric or meteoritic observations. There have been various modifications and developments in the methods to determine the abundances and neutrino fluxes. The recent development of abundances has led to the revision of solar metallicity value to a lower value than the earlier one. Solar model constructed with this lower abundance set leads to the properties which contradict with the helioseismic observations. This contradiction between the solar model predictions and helioseismology is called the 'Solar Abundance Problem'. Many solutions have been proposed to solve this problem, and only some of them have been

able to partially solve the problem but none of them provides a proper solution. Some of the solutions suggest the changes in the basic input physics and parameters such as the opacity tables and abundances correction. There is also a suggestion to include 3-D equations in the standard solar model and include rotation and other complex features in it. Other than these, accurate neutrino fluxes observation can also throw light upon the true abundances of some of the major elements most relevant for solar abundance problem such as C, N and O. Some exotic particle physics solutions including dark matter have also been proposed which will contribute as the extra energy transport inside the Sun and hence affect the solar model results and make them comparable to helioseismology. The importance of the solar heavy-element abundance does not merely lie in being able to model the Sun correctly, it is often used as the standard against which heavy-element abundances of other stars are measured. Hence the accurate study of the Sun helps us to determine the details of other stars for which we have very less observational details. Therefore, Sun can acts as a laboratory to test our new physics such as for exotic particles and helioseimology acts as a tool to probe the changes in the interior. Helioseismology or asteroseismology hence has been used in various ways to constrain the exotic particle physics such as determination of the mass or scattering cross-section or kinetic mixing parameter of dark matter or axions or hidden photons etc. We can also use asteroseismology to probe the Dark matter content in the various parts of the universe.

Here, in this review we try to throw some light upon all these concepts in sequence as follows: In Chapter 2, we try to build the stellar models using the basic equations and mention the input parameters required. We focus mainly on the Standard Solar model. Then we discuss the physics behind the stellar oscillations in chapter 3, the equations, their spherical approximations and their properties and classification into $p$ and $g$ modes i.e. the acoustic and gravity modes respectively. We mention the basic observation tools for the $p$-modes and the importance of the frequency separation ratios as a diagnostic tool for probing the stellar core. In chapter 4, we discuss about some of the observation techniques and how helioseismic observations can be inverted to determine the solar interior details. Then we throw some light upon the Solar abundance problem in chapter 5, and discuss the consequences of the new abundances and how they conflict with the helioseismology. In chapter 6, we propose some solutions to the problem including some of the general and some exotic particle physics solutions. We also discuss in chapter 7 about the constraints that have been put on the exotic particles using helioseismology or asteroseismology and finally, how they can be used to probe the Dark matter content of the universe in chapter 8.

# Chapter 2

# Making Stellar models

## 2.1 Equations of stellar structure

A star can be modeled under the assumption that it is a spherically symmetric object i.e. its internal structure is only a function of radius and not of latitude or longitude. This allows us to express its properties with a set of 1-D equations derived from basic principles with mass 'r' as the independent variable: [1, 2]

1. **Conservation of mass**
$$\frac{dM_r}{dr} = 4\pi r^2 \rho \tag{2.1}$$
where $M$ is the mass enclosed in radius $r$ and $\rho$ the density.

2. **Conservation of momentum or hydrostatic equilibrium**
$$\frac{dP}{dr} = -\frac{GM_r\rho}{r^2} \tag{2.2}$$
where $P$ is the pressure.

3. **Conservation of energy:** At equilibrium, luminosity $L_r$ is the energy flowing through a shell of radius $r$ per unit time as a result of nuclear reactions in the interior. If $\epsilon$ be the energy released per unit mass per second by nuclear reactions like pp chain and CNO chain, and $\epsilon_v$ the energy lost by the star because of neutrinos streaming out of the star without depositing their energy, $\epsilon_g$ (g for gravity) be the release of gravitational energy i.e. due to expansion (or contraction) of stellar layers we get:
$$\frac{dL_r}{dr} = 4\pi r^2(\epsilon + \epsilon_g - \epsilon_v) \tag{2.3}$$

4. **Energy transport:**
$$\frac{dT}{dr} = -\frac{GM_rT}{r^2P}\bigtriangledown \tag{2.4}$$
where $\bigtriangledown$ is the dimensionless 'temperature gradient' $(d\,ln\,T/d\,ln\,P)$ which depends on the mode of energy transfer, dominant ones are radiation and convection.

5. **Change of chemical composition with time:** Three main reasons for this are

   (a) Nuclear reactions: If $X_i$ is the mass fraction of any isotope i, then,

   $$\frac{\partial X_i}{\partial t} = \frac{m_i}{\rho}\left[\sum_j r_{ji} - \sum_k r_{ik}\right] \tag{2.5}$$

   where $m_i$ is the mass of the nucleus of each isotope $i$, $r_{ji}$ is the rate at which isotope $i$ is formed from isotope $j$, and $r_{ik}$ is the rate at which isotope $i$ is lost because it turns into a different isotope $k$ and is input to models.

   (b) Changing boundaries of convection zones: the rate at which $\overline{X}_i$ (average abundance of any species $i$ in the convection zone) changes will depend on nuclear reactions in the convection zone, as well as the rate at which the mass limits $M_1$ and $M_2$ of spherical shells change.

   (c) Diffusion and gravitational settling of helium and heavy elements:

   $$\frac{\partial X_i}{\partial t} = D\nabla^2 X_i \tag{2.6}$$

   where $D$ is the diffusion coefficient.

## 2.2 Scharzchild criterion of convection

$\bigtriangledown$ the 'temperature gradient' $(d\,ln\,T/d\,ln\,P)$ in the radiative zones, under the approximation of diffusive radiative transfer is given by

$$\nabla = \nabla_{rad} = \frac{3}{64\pi\sigma G}\frac{\kappa L_r P}{M_r T^4} \tag{2.7}$$

where, $\sigma$ is the Stefan-Boltzmann constant and $\kappa$ is the opacity.

In convective zones, $\nabla$ is usually the adiabatic temperature gradient

$$\nabla_{ad} \equiv (\partial\,ln\,T/\partial\,ln\,P)_s \tag{2.8}$$

($s$ being the specific entropy).

Whether energy is transported by radiation or by convection depends on the value of $\nabla_{\rm rad}$. 'Schwarzschild Criterion'[1] says that if

$$\nabla_{\rm rad} > \nabla_{\rm ad} \tag{2.9}$$

**convection** sets in.

## 2.3 Mixing length theory of Convection

Deep inside a star, the temperature gradient is well approximated by the adiabatic temperature gradient $\nabla_{\rm ad}$. This approximation cannot be used in the outer layers where convection is not efficient and some of the energy is also carried by radiation. So we propose an approximate formalism called '**Mixing Length Theory'(MLT)** [1] for convection . Here the heat is transported by macroscopic eddies and their mean free path is called the 'mixing length'. The main assumption is that the size of the convective eddies at any radius is the mixing length $l_m$, where

$$l_m = \alpha_{MLT} H_P \tag{2.10}$$

and $\alpha_{\rm MLT}$, a constant, is the 'mixing length parameter',and $H_P$ is the pressure scale height given by $-d\,r/d\,ln\,P$.

## 2.4 Inputs to stellar models

Other than the equations of stellar structure, we need some more input physics to model the stellar interior and its evolution. The input microphysics includes :[1]

1. **The Equation of State :** There are five equations in six unknowns, $M_r$, $P$, $L_r$, $T$, $X_i$, and $\rho$. So, we need one more equation relating these quantities i.e. equation of state. Among the popular equations of state used to construct solar models are the OPAL , MHD, and the CEFF equation of state.

2. **Opacity $\kappa$ :** Rosseland mean opacities are given in tabular form as a function of density, temperature and composition. Among the tables used to model the Sun are the OPAL tables , and the OP tables.

3. **Nuclear Reaction Rates** : are required to compute energy generation, neutrino fluxes and composition changes which are calculated either theoretically or are obtained by extrapolating laboratory measurements.

4. **Boundary Conditions : [2]**

   - as $r \longrightarrow 0$ : $M_r, L_r \longrightarrow 0$;
   - as $r \longrightarrow R_*$ : $T, P, \rho \longrightarrow 0$, where $R_*$ is the star's radius.

## 2.5 Standard Solar Model (SSM)

SSMs are one-dimensional evolutionary models of a $1\,M_\odot$ star, starting from a homogeneous model in the pre-main sequence up to the present-day age of the solar system $\tau_\odot = 4.57\,$Gyr. At this age, the model has to satisfy three observational constraints: [3]

1. the present-day luminosity $L_\odot = 3.8418 \times 10^{33}\,$ers s$^{-1}$
2. radius $R_\odot = 6.9598 \times 10^{10}\,$cm

3. $(Z/X)_\odot$, $Z$ is the metallic abundance and $X$ is hydrogen abundance of the Sun.

Three free parameters are calibrated to fulfill these conditions:

1. the mixing length parameter $\alpha_{\rm MLT}$
2. $Y_{\rm ini}$
3. $Z_{\rm ini}$.

The relative abundances of individual metals are assumed to be the same for a given $(Z/X)_\odot$. The initial hydrogen abundance is determined from the normalization $X + Y + Z = 1$.

Standard solar models constructed by different groups are not identical. They depend on the microphysics used, as well as assumption about the heavy element abundance.

By solving the stellar model equations and using the boundary conditions as in above sections, we can find the general trend of the variables $M_r$, $P$, $L_r$, $T$, and $\rho$. as a function of $r$. In figure 2.1, we show the schematic diagram of the Solar interior, it shows that nuclear reactions occur in the deep core and energy is transported through radiation in inner regions and through convection in outer regions i.e. $r > 0.714\,R_\odot$. Then in figure 2.2, 2.3, 2.4, we show the radial profile of the temperature, pressure, luminosity and its derivative, density and mass of the Solar interior.

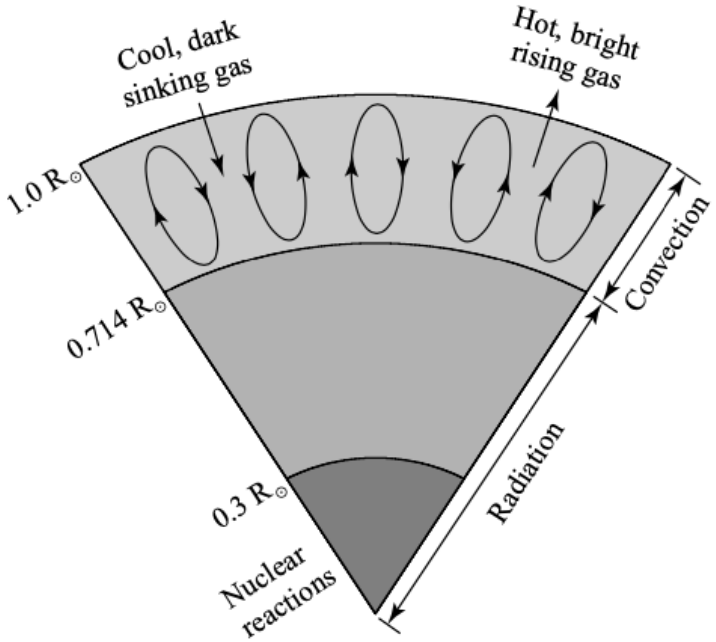


Figure 2.1: Schematic diagram for the Sun's interior. [2]

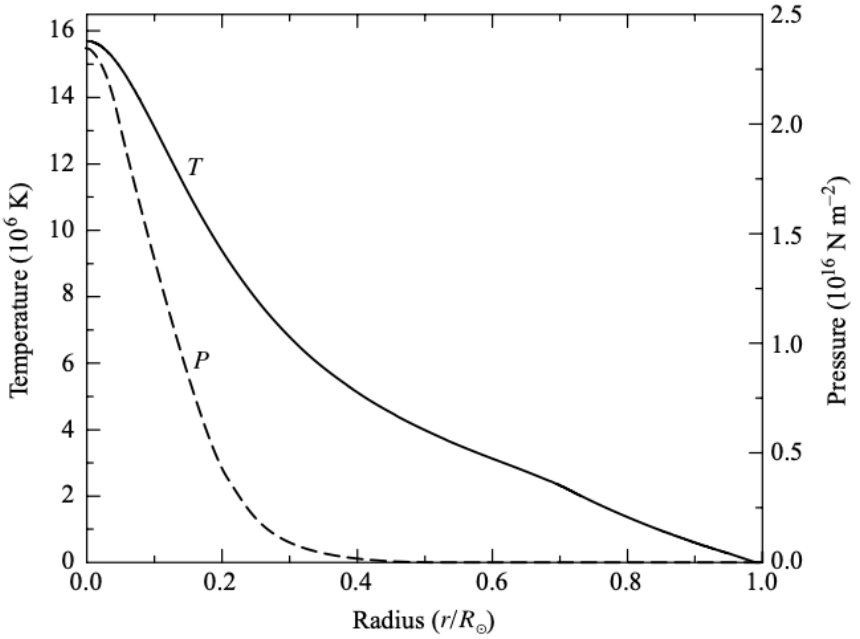


Figure 2.2: The Temperature (T) and Pressure (P) profiles in the Solar interior.(Data from Bahcall, Pinsonneault, and Basu, Ap. J, 555, 990, 2001.) [2]

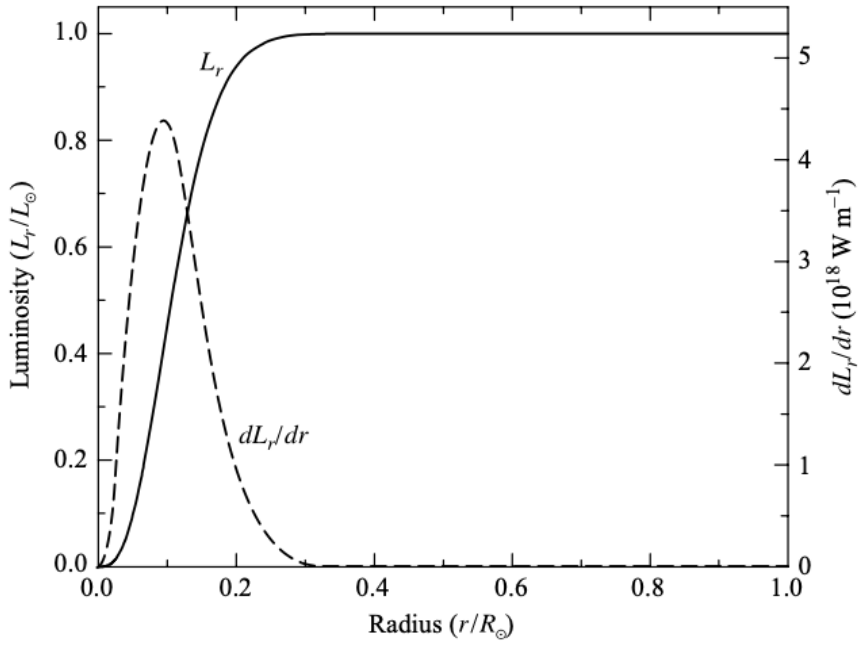


Figure 2.3: The interior luminosity profile of the Sun ($L_r$) and the derivative of the interior luminosity as a function of radius $r$. (Data from Bahcall, Pinsonneault, and Basu, Ap. J, 555, 990, 2001.)[2]

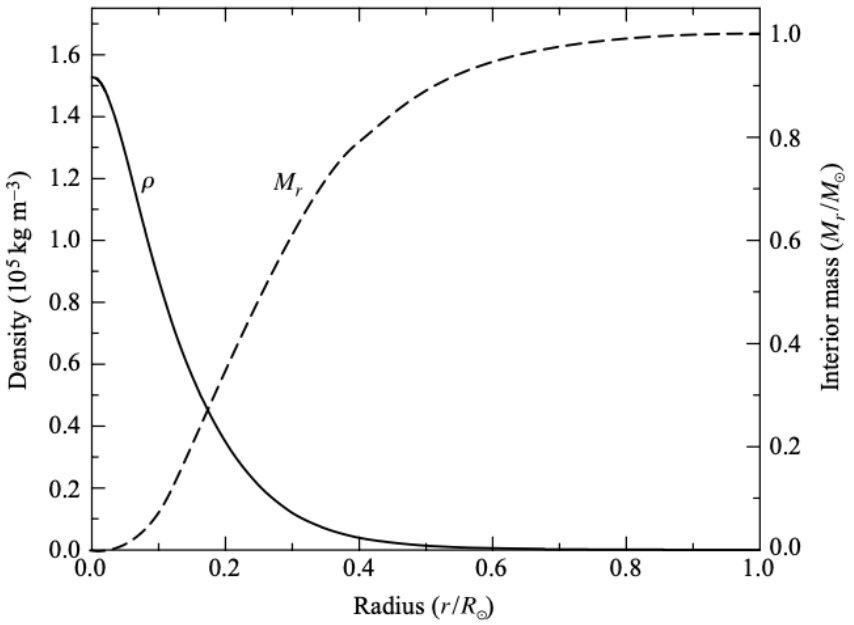


Figure 2.4: The density profile ($\rho$) and the interior mass of the Sun ($M_r$) as a function of radius $r$.(Data from Bahcall, Pinsonneault, and Basu, Ap. J, 555, 990, 2001.)[2]

# Chapter 3

# Stellar Oscillations

## 3.1 The Basic Equations

The stellar oscillations can be described by starting with the basic equations of fluid dynamics which are as follows:[4]

1. Continuity equation
$$\frac{\partial \rho}{\partial t} + \nabla.(\rho \mathbf{v}) = 0 \tag{3.1}$$

2. Momentum equation
$$\rho \left( \frac{\partial \mathbf{v}}{\partial t} + \mathbf{v}.\nabla \mathbf{v} \right) = -\nabla P + \rho \nabla \Phi \tag{3.2}$$

3. Poisson's equation to describe the gravitational field
$$\nabla^2 \Phi = 4\pi G \rho \tag{3.3}$$

4. Energy equation in adiabatic approximation
$$\frac{\partial P}{\partial t} + \mathbf{v}.\nabla P = c^2 \left( \frac{\partial \rho}{\partial t} + \mathbf{v}.\nabla \rho \right) \tag{3.4}$$

   where $\mathbf{v}$ is the velocity of the fluid element, $c = \sqrt{\Gamma_1 P/\rho}$ is the sound speed, $\Phi$ is the gravitational potential, and $G$ the gravitational constant and $\Gamma_1 = \left( \frac{\partial ln P}{\partial ln \rho} \right)_{ad}$.

If we perform linear perturbations of the above fluid equations we get the linear stellar oscillation equations. Thus, e.g., we can write eulerian perturbations to density as:

$$\rho(\mathbf{r}, t) = \rho_0(\mathbf{r}) + \rho_1(\mathbf{r}, t), \tag{3.5}$$

where the subscript 0 denotes the equilibrium, spherically symmetric quantity which by definition does not depend on time, and the subscript 1 denotes the perturbation. Perturbations to other quantities can be written in the same way. Velocity is given by $\mathbf{v} = \partial \overrightarrow{\xi} / \partial t$, where $\overrightarrow{\xi}$ is the displacement from equilibrium position.

Substituting the perturbed quantities in the equations above and keeping only linear terms in the perturbation, we get:

$$\rho_1 + \nabla \cdot (\rho_0 \overrightarrow{\xi}) = 0, \tag{3.6}$$

$$\rho_0 \frac{\partial^2 \overrightarrow{\xi}}{\partial t^2} = -\nabla P_1 + \rho_0 \nabla \Phi_1 + \rho_1 \nabla \Phi_0, \tag{3.7}$$

$$\nabla^2 \Phi_1 = 4\pi G \rho_1. \tag{3.8}$$

$$P_1 + \overrightarrow{\xi} \cdot \nabla P_0 = c_0^2 (\rho_1 + \overrightarrow{\xi} \cdot \nabla \rho_0) \tag{3.9}$$

Next we drop the subscript '0' for the equilibrium quantities, and only keep the subscript for the perturbations.

## 3.2 Spherically Symmetric case

Since Stars are usually spherical, we can write the different quantities and hence, the equations in terms of their radial(r) and tangential(_t) components in spherical-polar coordinates $(r, \theta, \varphi)$. We see that the new equations don't have mixed radial and tangential derivatives hence we can write tangential parts of the perturbed quantities in terms of the spherical harmonic functions $Y_l^m(\theta, \varphi)$ [4]. And since, time derivatives are explicit so we can separate the time dependence from the spatial part and can be expressed in terms of $e^{-i\omega t}$ where $\omega$ can be real (oscillations) or imaginary(exponential growth or decay). We can write:

$$\xi_r(r, \theta, \varphi, t) \equiv \xi_r(r) Y_l^m(\theta, \varphi) exp(-i\omega t), \tag{3.10}$$

$$P_1(r, \theta, \varphi, t) \equiv P_1(r) Y_l^m(\theta, \varphi) exp(-i\omega t), \tag{3.11}$$

etc.

When we put this into the equations we get 3 equations :

$$\frac{d\xi_r}{dr} = -\left(\frac{2}{r} + \frac{1}{\Gamma_1 P}\frac{dP}{dr}\right)\xi_r + \frac{1}{\rho c^2}\left(\frac{S_l^2}{\omega^2} - 1\right) P_1 - \frac{l(l+1)}{\omega^2 r^2}\Phi_1, \tag{3.12}$$

$$\frac{dP_1}{dr} = \rho(\omega^2 - N^2)\xi_r + \frac{1}{\Gamma_1 P}\frac{dP}{dr} P_1 + \rho \frac{d\Phi_1}{dr} \tag{3.13}$$

and

$$\frac{1}{r^2}\frac{d}{dr}\left(r^2 \frac{d\Phi_1}{dr}\right) = -4\pi G\left(\frac{P_1}{c^2} + \frac{\rho \xi_r}{g} N^2\right) + \frac{l(l+1)}{r^2}\Phi_1 \tag{3.14}$$

where $S_l^2$ is the *Lamb frequency* :

$$S_l^2 = \frac{l(l+1)c^2}{r^2} \tag{3.15}$$

and $N$ is Brunt-Väisälä or buoyancy frequency :

$$N^2 = g\left(\frac{1}{\Gamma_1 P}\frac{dP}{dr} - \frac{1}{\rho}\frac{d\rho}{dr}\right) \tag{3.16}$$

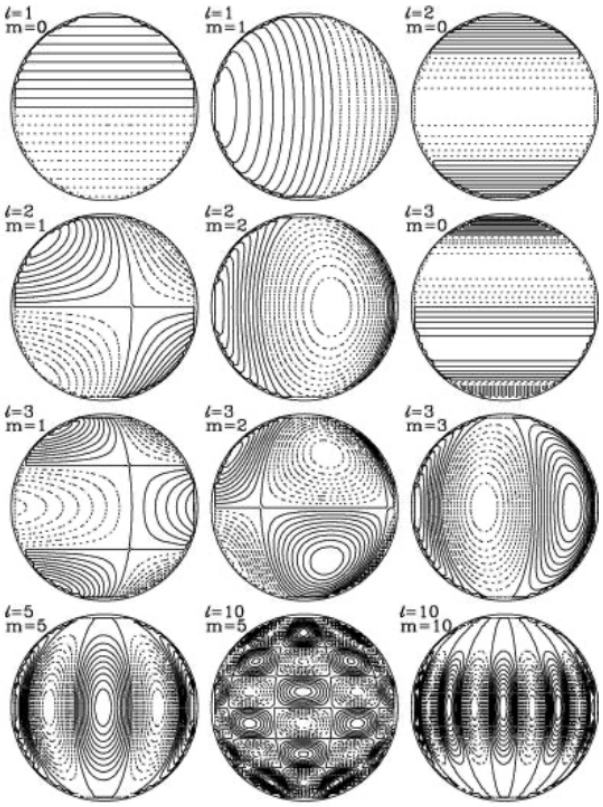


Figure 3.1: The Spherical harmonics $Y_l^m(\theta, \varphi)$ i.e. stellar oscillations on the surface of the star. Source :web.

It is the oscillation frequency of the fluid element disturbed from its equilibrium position. Regions where $N^2 < 0$, convective transport exists. These equations (3.12, 3.13, 3.14) when combined together form an **eigenvalue problem** with $\omega' s$ as the eigenvalues, each referred to as a "mode" of oscillation.

Since the equations are independent of $n$ and $m$, so, we can label eigenvalues of same $l$ (degree) with $n$ (order) i.e $\omega_{n,l}$. '$n$' can be any integer: positive, negative, zero depending on the mode and $|n|$ signifies the number of radial nodes of the radial eigenfunction. the degree '$l$' is related to the horizontal wavelength of the mode and is approximately the number of nodes on the solar surface and the azimuthal order $m$ defines the number of nodes along the equator.

- $n > 0$ : acoustic or $p$ modes
- $n < 0$ : gravity or $g$ modes
- $n = 0$ : fundamental or $f$ modes

and since, we are considering the spherically symmetric system so all modes for a given $n$, $l$ are degenerate in $m$.

## 3.3 Properties of Stellar oscillations

To understand the properties of stellar oscillations we try to approximate the equations (3.12, 3.13, 3.14) :

- Cowling approximation: perturbation to the gravitational potential $\Phi_1$ can be ignored where $|n|$ and $l$ are large,
- We assume that we are looking far away from center (i.e. large $l$) so $1/r$ terms neglected,
- We assume that variations in eigenfunctions is more rapid than equilibrium quantities for high $|n|$ oscillations hence terms containing $H_P^{-1}$ can be neglected where $H_P = -\frac{dr}{d\,ln\,P}$ is the pressure scale height.

Thus, we get a combined second order differential equation [4]

$$\frac{d^2\xi_r}{dr^2} = K(r)\xi_r \tag{3.17}$$

$$K(r) = \frac{\omega^2}{c^2}\left(1 - \frac{N^2}{\omega^2}\right)\left(\frac{S_l^2}{\omega^2} - 1\right) \tag{3.18}$$

We can see that the solution is oscillatory when:

1. $\omega^2 < S_l^2$, and $\omega^2 < N^2$ : **g modes** - trapped mainly in the core (figure 3.2) - restoring force is gravity through buoyancy,
2. $\omega^2 > S_l^2$, and $\omega^2 > N^2$ : **p modes** - generally oscillatory in outer regions (figure3.2) - restoring force is mainly pressure;

The solution is exponential otherwise.

## 3.4 $p$-modes

The $p$-modes are trapped between the surface and the inner turning point $r_t$ given by $\omega^2 = S_l^2$. For high frequency $p$ modes, i.e., modes with $\omega \gg N^2$

$$K(r) \simeq \frac{\omega^2 - S_l^2(r)}{c^2(r)}, \tag{3.19}$$

hence, their behavior is predominantly determined by the behavior of the sound-speed profile, which is pressure, i.e., sound waves ($n > 0$).

Figure 3.3 shows the non-radial $p$-modes for different degree and order. We observe that lower degree modes penetrate deeper into the core whereas higher degree modes have significant amplitude of oscillation close to the stellar-surface only. Thus, they allow a diagnosis of the conditions on the surface layers.

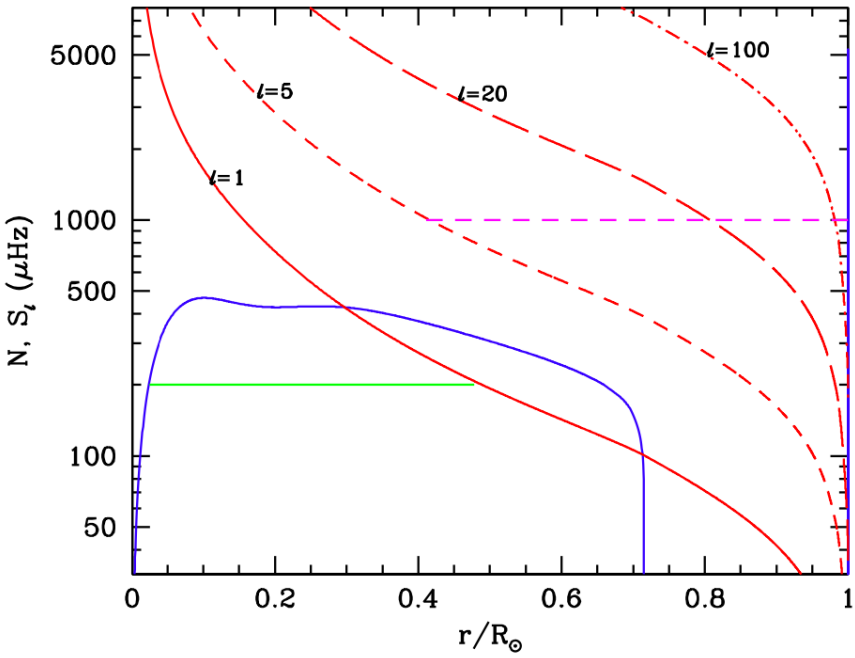


Figure 3.2: The propagation diagram for a standard solar model. The blue line is the buoyancy frequency, the red lines are the Lamb frequency for different degrees. The green solid horizontal line shows the region where a 200 μHz $g$-mode can propagate. The pink dashed horizontal line shows where a 1000 μHz $l = 5$ $p$-mode can propagate. Source: [4]

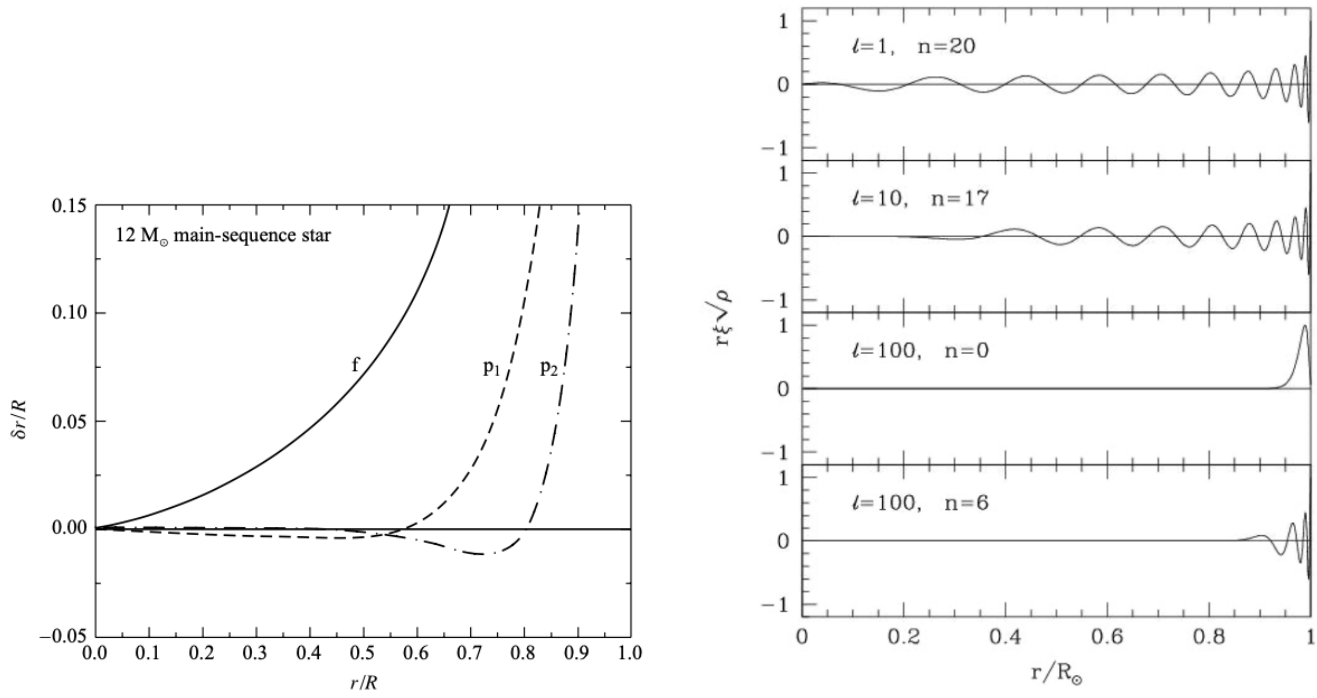


Figure 3.3: Non-radial $p$ modes with different $l$ are shown. In left figure, $l = 2$ and $f$ mode is also shown for 12 $M_\odot$ star. Source :[2] and web.

An asymptotic analysis of the equations for frequencies of high order($n$) and low-degree ($l$) $p$-modes ($n >> l$) can be written as:[4]

$$\nu_{n,l} \simeq \left(n + \frac{l}{2} + \alpha_p\right) \Delta\nu, \tag{3.20}$$

where

$$\triangle\nu_{n,l} = \left(2\int_0^R \frac{dr}{c}\right)^{-1} = \nu_{n+1,l} - \nu_{n,l} \tag{3.21}$$

is the **large frequency spacing** and $\alpha_p$ is the phase shift. We also have **small-frequency spacing** for low $l$ modes given by

$$\delta\nu_{n,l} = \nu_{n,l} - \nu_{n-1,l+2} \approx -(4l+6)\frac{\Delta\nu_{n,l}}{4\pi^2\nu_{n,l}}\int_0^R \frac{dc}{dr}\frac{dr}{c}, \tag{3.22}$$

The large frequency spacing is determined by the sound travel time from center to surface and hence has large contribution from near surface layers where sound speed is low. As a result, the large frequency spacing for models is affected by our inability to model the near-surface layers correctly. One way of reducing the effects of the near-surface errors is to use the so-called **frequency separation ratios** given by:

$$r_{0,2}(n) = \frac{\delta\nu_{n,0}}{\triangle\nu_{n,1}}, \tag{3.23}$$

$$r_{1,3}(n) = \frac{\delta\nu_{n,1}}{\triangle\nu_{n+1,0}} \tag{3.24}$$

These ratios represent the characteristics of the core and are not affected by the detailed structure of the solar surface, which is poorly described by stellar models. This is because for radial order $n \gg 1$ and low angular degree $l$, the surface effects are functions of the eigenfrequency, so they cancel out when considering frequency differences between modes of similar frequencies. In addition, by taking ratios of appropriate frequency differences, the core structure becomes the dominant effect in the observed signal. Hence, these ratios are very useful and can be used as a diagnostic tool to determine the properties and changes in the stellar core.

## 3.5 $g$-modes

In the case of the Sun the $g$ modes are trapped between the base of the convection zone and the core. The turning points of these modes are defined by $N = \omega$. For $g$-modes of high order, $\omega^2 \ll S_l^2$ and thus

$$K(r) \backsimeq \frac{1}{\omega^2}(N^2 - \omega^2)\frac{l(l+1)}{r^2} \tag{3.25}$$

hence its properties are dominated by the buoyancy frequency $N$.($n < 0$)

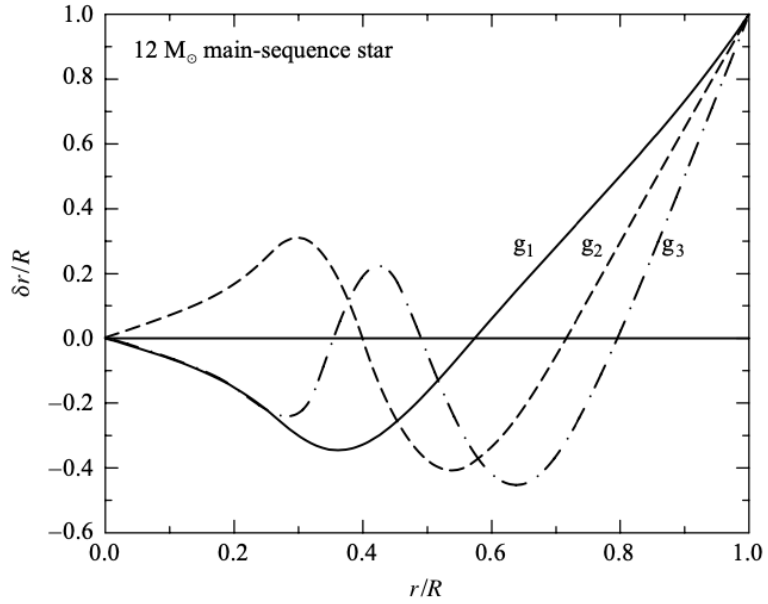


Figure 3.4: Non-radial $g$-modes with $l = 2$. Source:[2]

As shown in figure 3.4, non-radial $g$-modes involve significant movement of the stellar material deep within the star and hence provide details about the core of the star. However, $g$-modes are not yet detected for the Sun.

A complete asymptotic analysis of $g$-modes shows that the frequencies of high-order $g$-modes can be approximated as

$$\omega = \frac{\sqrt{l(l+1)}}{\pi(n + l/2 + \alpha_g)} \int_{r_1}^{r_2} N \frac{dr}{r} \tag{3.26}$$

where $\alpha_g$ is a phase that varies slowly with frequency. This shows that while $p$-modes are equally spaced in frequency, $g$-modes are equally spaced in period.

# Chapter 4

# Helioseismology

Helioseismology is the study of the interior of the Sun using Solar oscillations. In general, study of the interior of a star using its stellar oscillations is called **Asteroseismology**. Helioseismology can be used to determine the sound speed, density and adiabatic index profile of the Sun. Inversions of solar oscillations frequencies have allowed us to determine a number of other facts like the position of the base of the convection zone, Helium abundance in the convection zone, and, also the rotational profile of the Sun as a function of depth.

## 4.1 Observation Techniques

One can observe the oscillations in either the line of sight velocity via Doppler shift or in Intensity. Observations at surface can be written as:

$$v(\theta, \phi, t) = \sum_{l,m} a_{l,m}(t) Y_l^m(\theta, \phi) \tag{4.1}$$

so, we can perform the spherical harmonic transform of the observations which gives $a_{l,m}(t)$. Then, Fourier transform the spectrum and its peaks will give the frequencies of different modes $\nu_{n,l,m}$ ( figure 4.1). In absence of rotation and magnetic field $\nu_{n,l,m}$ is independent of $m$, while rotation lifts the degeneracy giving rotational splitting of modes.

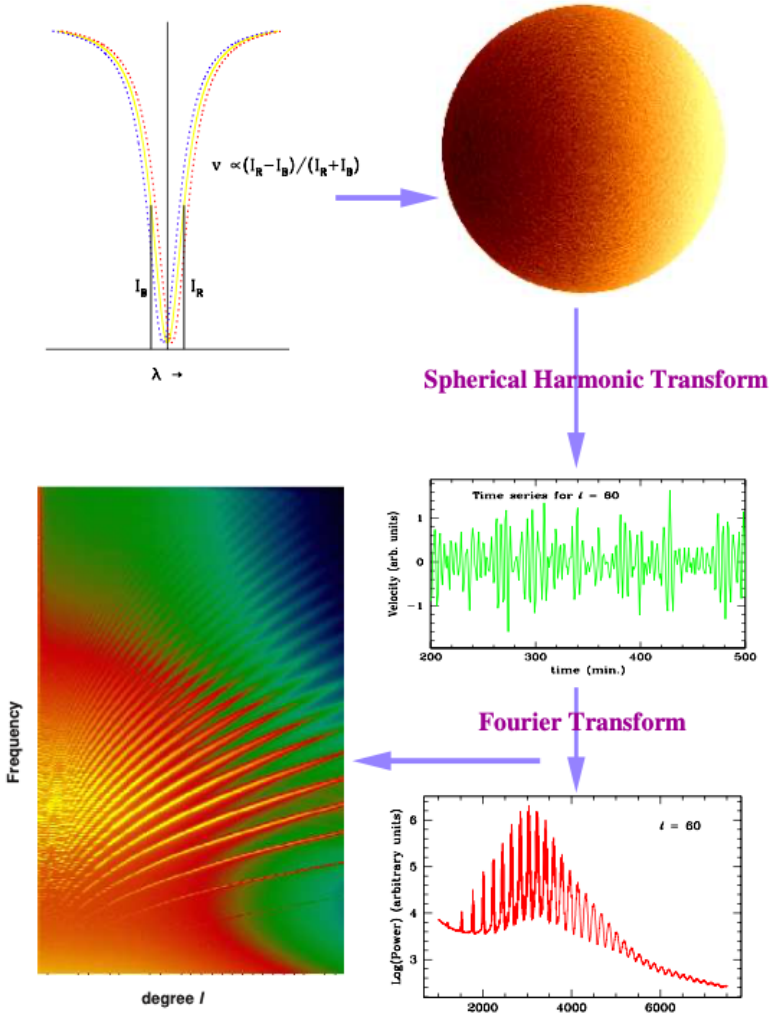


Figure 4.1: observation technique

## 4.2 Inversion Techniques

**Helioseismic Inferences** can be classified into two categories as:

1. Forward Technique : Compare frequencies of different models with observed frequencies. For e.g. estimating $R_{CZ}$- depth of the convection zone

2. Inverse technique : Using the observed frequencies, infer the internal structure or dynamics. For e.g., sound speed profile $c(r)$.

**Helioseismic Inversions:[1]**

Since the frequencies of acoustic modes depend mainly on the sound speed and density in solar interior, it is possible to invert the frequencies to obtain the sound speed $c$, and density $\rho$ . It can be shown that $c$, $\rho$ along with hydrostatic equilibrium are enough to determine the

solar model as far as frequencies are concerned. Pressure $p$ and adiabatic index $\Gamma_1$ can be determined from $c$, $\rho$. For this, the eigenvalue problem obtained by combining the equations (3.12, 3.13, 3.14) of the form:

$$L\overrightarrow{\xi}_{n,l} = -\omega^2\overrightarrow{\xi}_{n,l} \tag{4.2}$$

$L$ being a differential operator which is Hermitian under the boundary condition, $\rho = P = 0$ at the outer boundary. Hence we can apply the variational principle to linearize the eq 4.2 around a known solar model (called the "reference model") to obtain:

$$\delta\omega^2_{n,l} = -\frac{\int_V \rho\,\overrightarrow{\xi}^*_{n,l}.\delta L.\overrightarrow{\xi}_{n,l}dV}{\int_V \rho\,\overrightarrow{\xi}^*_{n,l}\overrightarrow{\xi}_{n,l}dV} \tag{4.3}$$

where $\delta\omega^2_{n,l}$ is the difference in the squared frequency of an oscillation mode of the reference model and the Sun, $\delta L$ is the perturbation to the operator $L$.

Perturbing the model yields the equation for inversion that relate the frequency differences between the Sun and the solar model to the differences in structure as:

$$\frac{\delta\nu_{n,l}}{\nu_{n,l}} = \int_0^R K^{n,l}_{c^2,\rho}(r)\frac{\delta c^2}{c^2}(r)dr + \int_0^R K^{n,l}_{\rho,c^2}(r)\frac{\delta\rho}{\rho}(r)d + \frac{F(\nu_{n,l})}{E_{n,l}} \tag{4.4}$$

where last term is the surface correction term and, $\delta c^2/c^2$ and $\delta\rho/\rho$ are the relative differences in the squared sound speed and density between the Sun and the model. The functions $K^{n,l}_{c^2,\rho}(r)$ and $K^{n,l}_{\rho,c^2}(r)$ are the kernels of the inversion that relate the changes in frequency $\rho, c$ to the changes in $c^2$ and $\rho$ respectively. These are known functions of the reference solar model.

To determine $\delta c^2/c^2$ and $\delta\rho/\rho$ from this, there are 2 methods:

1. **Regularized Least Squares method (RLS)** : Expand $\delta c^2/c^2$, $\delta\rho/\rho$, $F(\nu)$ in terms of suitable basis functions and the coefficients of expansion are determined by fitting the given data.

2. **Optimally Localized Averages method (OLA)** : a linear combination of the kernels is obtained such that the combination is localized in space. The solution obtained is then an average of the true solution weighted by the averaging kernel.

One can also compare the cores of solar models and that of the Sun using the frequency separation ratios $r_{0,2}$ and $r_{1,3}$ as defined earlier.

## 4.3 Determining Solar Helium Abundance ($Y_S$)

The adiabatic index $\Gamma_1$ is sensitive to the helium abundance in the helium ionization zones which lie in solar convection zone, and since the convection zone is well mixed, the helium abundance can be determined from $\Gamma_1$ and is the abundance throughout the solar convection zone.

The reduction in $\Gamma_1$ in the ionization zones also affects the sound speed which can be seen through the dimensionless gradient of the sound speed, $W(r)$, where

$$W(r) = \frac{1}{g}\frac{dc^2}{dr}, \tag{4.5}$$

and $g$ is the acceleration due to gravity. The peak around $r = 0.98R_\odot$ in the plot of $W(r)$ ( figure 4.2 )as a function of $r$ in the Sun is due to the $HeII$ ionization zone. This peak can be calibrated to find the helium abundance.

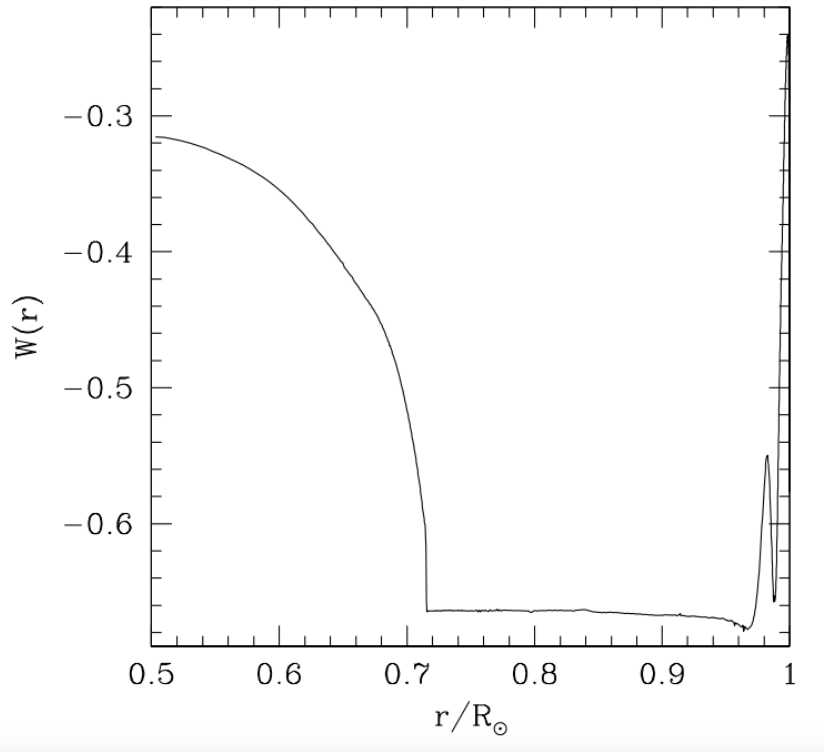


Figure 4.2: The dimensionless gradient of sound speed, $W(r)$, of a solar model plotted as a function of radius. [1]

## 4.4 Determining the depth of the Solar Convection Zone ($R_{CZ}$)

The base of the convection zone is the layer where the temperature gradient switches from the adiabatic value inside the convection zone to the radiative value below the convection zone. This introduces a discontinuity in the second derivative of the temperature and hence, the sound speed, which results in a discontinuity in the gradient of $W(r)$. The position of this discontinuity can be determined to estimate the convection zone depth

Otherwise, the abrupt change in the temperature gradient, at $R_{CZ}$ results in a large change in the sound-speed difference between two models that have different values of $R_{CZ}$.

This difference can be calibrated to determine the position of the solar convection-zone base.4.3

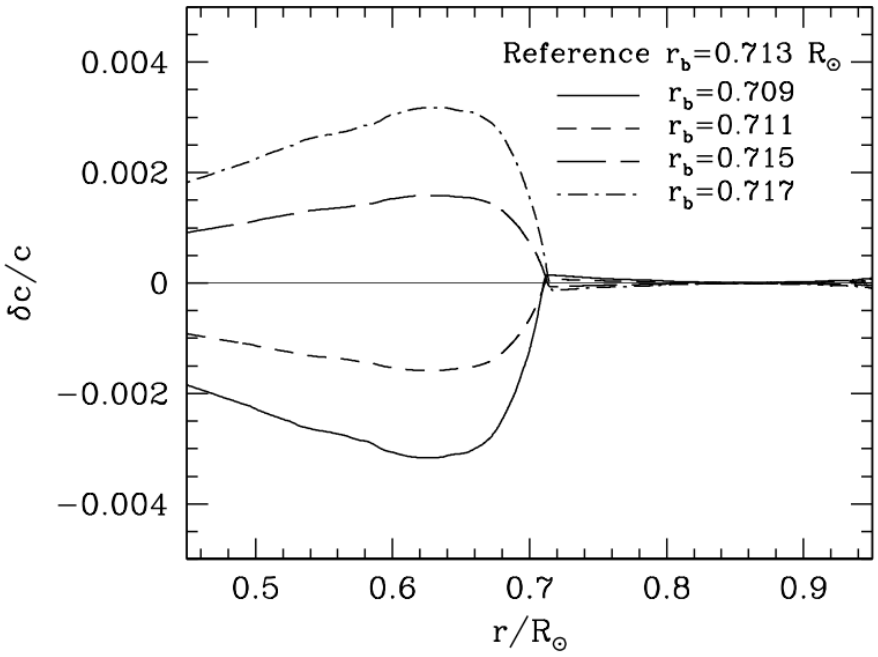


Figure 4.3: The relative sound-speed difference between a model with a convection-zone base at $R_{CZ} = r_b = 0.713 R_\odot$ and models with convection zone bases at different positions. Source: [1]

# Chapter 5

# Solar Abundance Problem

## 5.1 Introduction

The Solar metallicity $Z$ is one of the most important inputs to the solar models as it affects the microphysics inputs like opacity, equation of state, and nuclear energy generation rate. hence, different solar compositions provide different details of the solar interior which conflicts with the helioseismology.

Therefore, the conflict between the helioseismic observations of solar interior and the predictions made by the standard solar model using the new solar abundances obtained by 3-D and NLTE models of radiative transfer which have low heavy element abundance $Z$ is referred to as the **Solar Abundance problem**.

## 5.2 Methods to determine elemental abundances

Different methods can be classified as[3]

- **Empirical and semi-empirical methods** : the analysis of the observed solar spectrum, from the IR and optical (photospheric spectrum) to X-Ray (corona), sunspots, measurements of the solar wind, flares, and energetic particles.,chemical analysis of $Cl$ chondritic meteorites for refractory metals.

- **theoretical methods** : inversions of helioseismic data and nucleosynthesis models for heavy noble gases .

The reference element **Si** is used to convert abundances obtained from different methods to the same scale. Abundances from solar wind, corona, flares, or sunspots are converted to the photospheric scale using Ne/Mg or Ne/O ratios.

Specific methods used for the analysis of different element groups are:

- **He** abundance can be inferred from the solar wind and corona or from helioseismic inversions,

- light elements **Li, B,** and **B** are determined from the solar spectrum,

- volatile elements **C, N, O** can be determined from the solar coronal and photospheric spectrum which are model dependent.
- **refractory elements** can be determined from meteorites and from the solar photospheric spectrum.
- **Kr** and **Xe** are determined from nucleosynthesis models of slow-neutron capture process.

## 5.3 Solar Abundances

Earlier, solar abundances have been determined from the photospheric spectrum using the one-dimensional (1-D) atmospheric models adopting Local Thermodynamic Equilibrium (LTE), For e.g., the Standard Solar Composition (SSC) based on this method is **GS98** [5].

The recent developments in the methods of stellar spectroscopy has allowed to perform three-dimensional (3D) radiation hydrodynamics (RHD) simulations and adopt non-LTE radiation transport models to obtain new set of abundances. For e.g., **AGSS09** [6].

The difference in abundances in log scale of different elements for the two sets is shown in figure 5.1 .

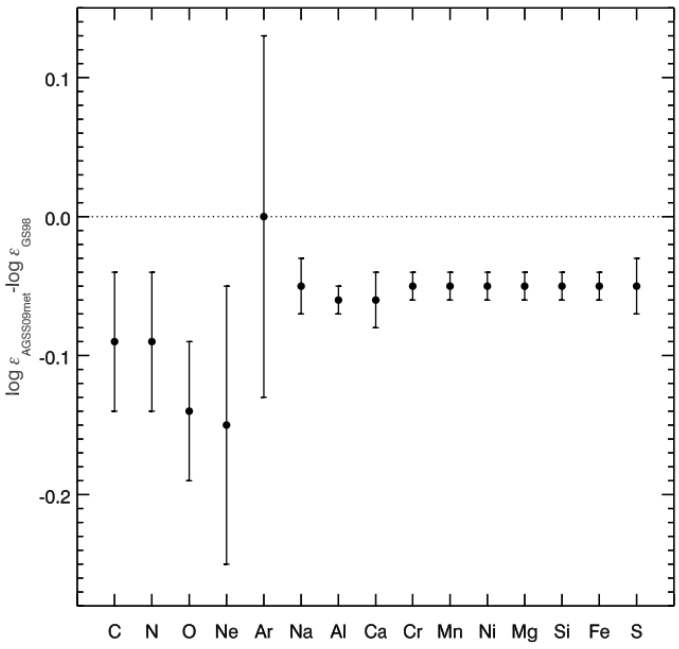


Figure 5.1: Difference between AGSS09 and GS98 solar abundances in log scale. Elements shown here are the most relevant for solar model calculations. Photospheric abundances for the volatile elements and meteoritic abundances for all other elements in both sets of abundances are used. Source :[3]

### 5.3.1 AGSS09 and GS98

As can be seen in figure 5.1, AGSS09 abundances are systematically lower than the older GS98 values and the most relevant element differences in the two abundances amount to 20% to 40% for CNO, Ne and 12% for refractories (Na, Al, Ca, Cr, Mn, Ni, Mg, Si, Fe, S). The metal-to-hydrogen mass ratio $(Z/X)_\odot$ are:

$$(Z/X)_{\mathrm{GS98}} = 0.0229; (Z/X)_{\mathrm{AGSS09}} = 0.0178. \tag{5.1}$$

The main results obtained from the SSM using the two abundances namely, GS98 and AGSS09 along with the solar (helioseismic) results are given in the table 5.1 in which $\langle \delta c/c \rangle$ and $\langle \delta \rho/\rho \rangle$ are the average root-mean-square deviations of the relative difference between the model (SSM) and the solar (helioseismic) quantities. Figure 5.2 also shows the relative differences of the sound speed profile and of the mean density profile for both models as a function of R.

| | $(Z/X)_\odot$ | $Z_\odot$ | $Y_S$ | $R_{CZ}/R_\odot$ | $\langle \delta c/c \rangle$ | $\langle \delta \rho/\rho \rangle$ | $Z_{ini}$ | $Y_{ini}$ |
|---|---|---|---|---|---|---|---|---|
| GS98 | 0.0229 | 0.0170 | 0.243 | 0.712 | 0.0009 | 0.011 | 0.0187 | 0.272 |
| AGSS09 | 0.0178 | 0.0134 | 0.232 | 0.723 | 0.0037 | 0.040 | 0.0149 | 0.262 |
| Solar | 0.0229/0.0178[a] | 0.0168/0.0131[a] | 0.2485[b] ±0.0035 | 0.713[b] ±0.001 | 0(def) | 0(def) | — | — |

Table 5.1: Main characteristics of the SSM- GS98 and AGSS09 and comparison to the solar (helioseismic) results. [a]refers to the GS98/AGSS09 abundances. Source: [3]

## 5.4 Consequences of different abundances

From table 5.1 we see that the GS98 SSM agrees well with the helioseismic inferences for $Y_S$, and $R_{CZ}$, whereas AGSS09 SSM differs by a lot. Therefore, we can see from the differences in the initial mass fractions of helium and of metals, $Y_{\mathrm{ini}}$ and $Z_{\mathrm{ini}}$, that $(Z/X)_\odot$ has a direct impact on the calibration of the solar model.[3]

The primary effect of the metallicity $Z$ is on the radiative opacity $\kappa$ in the solar interior as it determines the temperature gradient in the radiative region. The effects on different quantities can be shown as:

- $\mathbf{R_{CZ}}$ : A lower metallicity leads to a smaller temperature gradient in the radiative region and, by virtue of the Schwarzschild convection criterion, a shallower depth of the convective envelope $R_{CZ}$.
- $\boldsymbol{\delta c/c}$ : In the convective envelope (grey area, 5.2), where the temperature gradient does not depend on $\kappa$, but only on the equation of state, both the GS98 and AGSS09 models agree well with the seismic data, $\delta c/c \sim 0$. However, in the radiative zone, where $\kappa$ affects the solar structure, differences in the sound speed profiles show up.

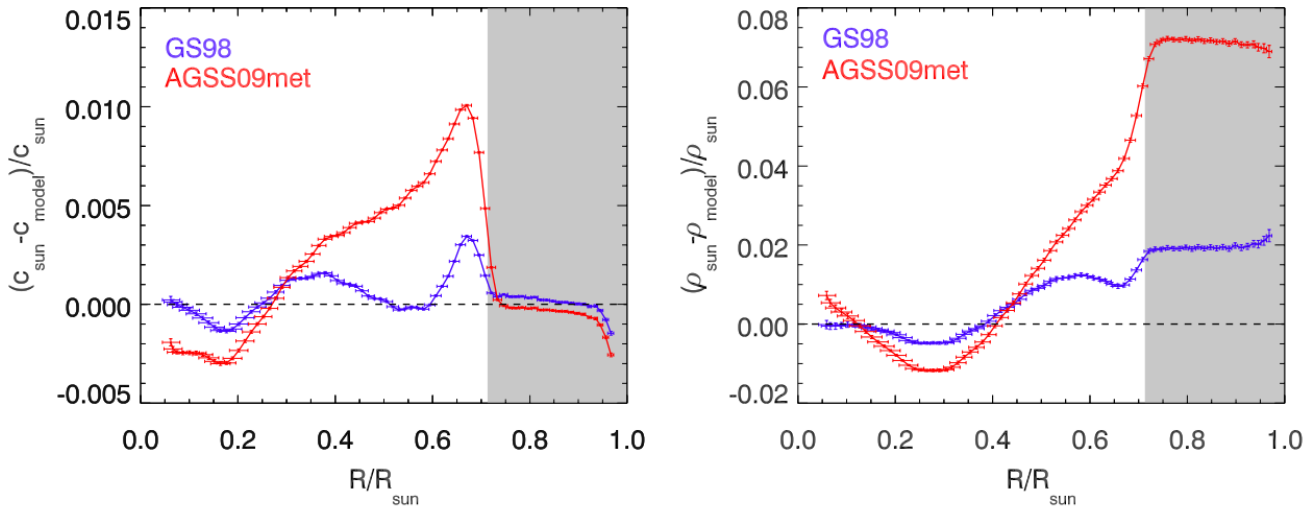


Figure 5.2: Profiles of the relative difference in sound speed (left panel) and density (right panel) between the Sun and two SSMs. Models are labeled according to the SSC that was adopted in the calibration of the SSM. The grey area denotes the solar convective envelope. The error bars reflect the uncertainties from the helioseismic data. Source: [3]

- $\delta\rho/\rho$ : Since, the density profile is constrained by the total mass of the Sun, the density values at different radii are correlated. Therefore, smaller density difference between the Sun and the model $\delta\rho/\rho$ in deep regions of high density are compensated by large density differences in the convective region.

- $\mathbf{Y_S}$ : lower opacity and shallower temperature gradient and thus a lower core temperature decreases the rate of nuclear energy generation. But, since nuclear reactions are the only relevant energy source in the Sun, so, we need to compensate for the decrease in temperature so that the fusion of hydrogen still produces energy at the same rate as the solar luminosity $L_{\odot}$ has to be constant,. This is achieved by the increase of hydrogen abundance or, equivalently, by the decrease of helium abundance. Therefore, we have lower $Y_S$ in the AGSS09 SSM which conflicts with helioseismology.

# Chapter 6

# Possible Solutions to Solar Abundance Problem

There have been numerous attempts to solve the Solar Abundance Problem. Here, we discuss some of the possible solutions and related papers on those topics. The solutions are basically classified as general solutions where attempts are made to change the inputs to solar models to get the right metallicity. Also, the Solar neutrino observations which can help to solve the problem by giving accurate abundances. Then, we discuss about changing the solar model by adding the extra energy transport factor in general or through dark matter.

## 6.1 General Solutions

### 6.1.1 Accuracy of radiative opacities

In the Solar models, the opacity profile is deduced from the atomic opacity calculations and a given Solar abundances. Therefore, to compensate for the decreased metallicity we can increase the opacities as they are the theoretical calculations of interaction of atoms and radiation in extremely dense physical environments [3]. In fact, it has been shown that an increase in the radiative opacities in the range of 15 to 20% at the base of the convective zone, smoothly decreasing to 3 to 4% in the solar core, would suffice to reconcile AGSS09 composition with the helioseismic results [7]. But, there is no experimental data to support these calculations. This, degeneracy between opacity and metallicity can be lifted by the Solar-neutrino measurements. As, the neutrino fluxes of CN-cycle are linearly dependent on the C and N abundances in the solar core. So, if we can measure the neutrino fluxes then we can determine their accurate abundances independent of their effect on opacities. (section 6.2)

### 6.1.2 Enhanced Gravitational Settling

Gravitational settling is a slow segregation process of chemical elements due to the combined effect of electric and gravitational field. In the Sun, settling rates are approximately similar for all metals and Helium. Due to this the solar surface metallicity and helium abundance at

present are lower than the initial values. To solve the problem, we need to increase the heavy-element abundance at the base of the convection zone and the radiative interior. This can be done relatively easily if it is assumed that diffusion and gravitational settling of helium and heavy elements is more efficient than what is normally assumed. Increased diffusion would lead to higher helium and heavy element abundance in the radiative interior, thereby increasing opacities and thus bringing the structure of radiative interior closer to that in the Sun. But, Such an ad-hoc solution is not sufficiently justified and should be avoided.[1]

### 6.1.3 Solar models with accretion of metal-poor materials

It was suggested that if we consider that a part of the disk, partially depleted in metals, is accreted onto the young Sun, then the solar interior will have a higher metal content than the envelope, this may solve the discrepancy [3]. They found that these models have a better agreement with helioseismology, as compared to normal AGSS09 models, but also found a spike in $\delta c^2/c^2$ just below the convection zone that is as large as 3.4%. Furthermore, both the convection-zone depth and the helium abundance in this model are lower than the corresponding seismically determined values.

### 6.1.4 Enhanced Solar neon abundance

'Ne' contributes to the radiative opacity at the base of the convective envelope and it has been found that if we increase its abundance by a factor of 2, we can solve the problem as it can compensate for the decreased Oxygen abundance [3]. The determination of Neon abundance is indirect i.e. through the coronal Ne/O ratio, by assuming the same ratio is present in the solar photosphere. As coronal models are uncertain, the abundance of neon is quite uncertain, justifying models with increased neon abundance. But, it was found that while increasing neon abundance reduces the discrepancy at the convection-zone base, it does not reduce the discrepancy in the ionization zones within the convection zone, rather increases the discrepancy in the region 0.75–0.9$R_\odot$.

### 6.1.5 Non Standard Solar model

SSM is a simplified picture of the actual Sun and its evolution. It does not account for the rotation, internal magnetic fields and the transport of angular momentum in the solar interior which might have measurable consequences in the solar structure. So, if we account for these processes in non-SSM we might be able to solve the problem. But, to model these processes is a multi-dimensional problem and is not feasible with present computational capabilities. Their simplified applications to 1-D models have been implemented but they contain new free parameters that have to be tuned to reproduce various observables, losing their predictive power. Also, such models based on the GS98 composition give an overall description of the solar structure that is worse than SSM results using AGSS09. Therefore, for non-SSM solution it is not yet possible to include realistic description of dynamical processes in the solar interior. [3]

### 6.1.6 Solar Wind Abundances

Another attempt to solve the problem was made in the paper [8] in which the new set of abundances of von Steiger & Zurbuchen 2016, determined through the in situ collection of solar wind samples from polar coronal holes are considered. It has the solar metallicity $Z_{\odot} \geq 0.0196 \pm 0.0014$, significantly higher than the currently established value. These new values of volatile elements (i.e. C, N, O, Ne) are close to the results of GS98, and those of refractory elements (i.e. Mg, Si, S, Fe) are considerably increased. They used the Linear Solar Model formalism, to determine the variation of helioseismological observables in response to the changes in elemental abundances, in order to explore the consistency of these new measurements with constraints from helioseismology.

They found that for the observables which are most sensitive to the abundance of volatiles (that is, sound speed and radius of CZB) the discrepancy of the model with the helioseismology is reduced whereas observables which are most sensitive to the abundance of refractories (that is, surface Helium abundance and neutrino fluxes) are predicted significantly larger than that inferred from helioseismology. So, the results indicate that, that these vSZ16 abundances studied in the Linear Solar Model do not solve the "solar abundance problem".

## 6.2 Neutrino Observations

The Sun is powered by nuclear fusion reactions occurring in its core. Each heavier element is produced through nuclear fusion from the lighter ones in a chain-reaction, with some steps in the chain releasing neutrinos of a characteristic energy spectrum. There are two main chains which convert hydrogen to helium in stars: the proton-proton chain and the carbon-nitrogen-oxygen (CNO) cycle, both of which lead to neutrino production. For the proton-proton chain there are five neutrino components (pp, $^{7}Be$, $^{8}B$, pep and hep) each with a different spectrum, while for the CNO cycle there are three ($^{13}N$,$^{15}O$ and $^{17}F$), and we refer to the sum of the latter as the CNO neutrinos.

We know that the observations of neutrino fluxes generated in CNO cycle in the interior of the Sun can provide accurate abundances of C, N and O independent of their opacities and hence help to resolve the solar abundance problem. So, here we discuss about some of the papers which talk about the experiments and their attempts to make the observations.

### 6.2.1 CNO Neutrino Grand Prix

Several next-generation experiments aim to make the first measurement of the neutrino flux from the Carbon-Nitrogen-Oxygen (CNO) solar fusion cycle. So, in this work [9] they try to determine the accuracy to which these future experiments can measure the CNO neutrino flux and time-scale for when the CNO flux will be measured with enough precision to tell us the metal content of the Sun's core, and thereby help to solve the solar metallicity problem.

For experiments looking at **neutrino-electron scattering**, they found that SNO+ will measure this CNO neutrino flux with enough precision after five years in its pure scintillator mode, provided its $^{210}Bi$ background is measured to 1% accuracy. By comparison, a 100 ton liquid argon experiment such as Argo will take ten years in Gran Sasso lab, or five years in

SNOLAB or Jinping. For Borexino ten years would be needed, but this projection is very sensitive to background assumptions.

For experiments looking at **neutrino- nucleus scattering**, the best prospects are obtained for low-threshold solid state detectors (employing either germanium or silicon). These would require new technologies to lower the experimental threshold close to detection of single electron-hole pairs, and exposures beyond those projected for next-generation dark matter detectors.

### 6.2.2 Sensitivity to CNO neutrinos in Borexino

We discuss the sensitivity of Borexino to CNO neutrinos based on the work [10]. Here, they tried to determine the two main residual background components: $^{210}Bi$ contamination, which can be estimated using measurements of $^{210}Po$ decays , and pep neutrinos and presented the strategy to constrain the backgrounds, the influence of additional purification of the liquid scintillator, and the possible sensitivity without an estimation of the $^{210}Bi$ contamination. They also tried to combine the measurement of the CNO neutrino flux with existing $^{7}Be$ and $^{8}B$ data with the Sun's surface metallicity to discriminate among SSMs.

### 6.2.3 Anticipating the Sun's metallicity through CNO neutrino flux

The elements C, N and O constitute the majority of the heavy elements in the Sun and their measurement through the CNO neutrino flux $\Phi_{CNO}$ will permit a crucial determination of the heavy-element abundance $Z_c$ in the Sun's energy-generating **core.** We need to determine the relation between $Z_c$ and $\Phi_{CNO}$ and from [11] we get it as

$$Z_c = \alpha \Phi_{CNO} \tag{6.1}$$

where $\alpha = 0.400$ and $\Phi_{CNO}$ is in units of $10^{10}$ c$^{-2}$ s$^{-1}$ . The uncertainty in $\alpha$ is dominated by uncertainties in the nuclear reaction rates.

Unlike hydrogen and helium abundances, the total CNO abundance is unaltered by the nuclear reactions, so the relation between $Z_c$ and the heavy-element abundance Z throughout the radiative envelope is relatively secure, depending only on the weak variation resulting from gravitational settling. Hence one can be assured that the analysis leading to this relation is reliable.

### 6.2.4 Helioseismic and Neutrino Data Driven Reconstruction of Solar Properties

Bayesian parameter inference and Gaussian process (GP) is used for non-parametric functional reconstruction of the radial opacity profile independently of any reference opacity tables, using the helioseismic and neutrino data to better determine the solar chemical composition and other solar properties (as well as their uncertainties) which are relevant to the solar abundance problem. When this method was applied to the two SSMs (GS98 and AGSS09), they found that allowing for the most flexible GP form of the opacity uncertainty profile decreases the evidence against the AGSS09 model but it is still strongly disfavoured.[12]

## 6.3 Generic energy transport solutions

In the paper [13], they considered the non-diffusive energy transport solutions to the problem. They combined the data from helioseismology, spectroscopy and solar neutrino detection experiments and calculated the additional energy flux inside the Sun. They found that a localized loss of energy near the radiative zone boundary and a gain of approximately the same amount of energy inside the solar core ($0.1R_\odot < r < 0.3R_\odot$) can solve the problem.

They showed that the localized loss of energy can be associated with the resonant emission of transversely polarized hidden photons, as long as the energy loss is compensated by energy deposition inside the core. They introduced then the light dark fermions coupled to hidden photons and discussed their interactions with the solar plasma and found the distribution of these dark particles inside the inner part of the radiative zone which is required to provide the necessary heating of the core.

### 6.3.1 Generalized form factor dark matter solutions

To try to solve the problem, we can consider the presence of asymmetric dark matter in the Sun which will affect its energy transport. In the paper [14], they considered the dark matter nucleon scattering cross-section proportional to $v^{2n}$ and $q^{2n}$ with $n = -1, 0, 1$ or 2, where $v_{rel}$ is the dark matter-nucleon relative velocity and $q$ is the momentum exchanged in the collision. Both spin-independent (SI) and spin-dependent (SD) dark matter capture were considered and their impact on the solar observables such as solar neutrino rates, the sound speed profile, convective zone depth, surface helium abundance and small frequency separations ($r_{02}$, $r_{13}$) was calculated by modelling the Sun using the hybrid code **DarkStec** and using the AGSS09 abundances for all 14 cases.

They observed that the impact of different types of generalized form factor DM on solar observables is quite varied, and not always straightforward. They found that the best improvement comes from a 3–5 GeV DM particle with SI cross-section given by $\sigma_{\rm SI} \propto q^2$ and it yields more than a $6\sigma$ improvement with respect to standard solar models, while being allowed by direct detection and collider limits. [15]

# Chapter 7

# Constraints on exotic particle physics with Asteroseismology

The ability of asteroseismology to probe the stellar interior in detail can be used to use the stars as laboratories for testing the new physics. If we consider the role of exotic particles in the stellar interior and hence in stellar evolution by considering their contribution to the stellar models then they will affect the asteroseismic and other observations as well. So, through asteroseismic and neutrino observations for different stars we can put constraints on exotic particle physics and here we discuss some of such attempts.

## 7.1 Dark matter in the Sun: scattering off electrons vs nucleons

When the dark matter present in the Sun annihilates it produces a flux of neutrinos which can be potentially detected with neutrino detectors/telescopes and the observations can be used to constraint the DM elastic scattering cross section. The process of capture of DM in Sun can be to be due to interactions with nucleons as well as electrons in specific scenarios. In this work [16], they have considered DM scatterings off electrons and have studied the capture, annihilation and evaporation processes entering the calculation of the neutrino production rates from DM annihilations in the Sun for three type of generic interactions: constant(velocity-independent and isotropic), $v_{rel}^2$-dependent(and isotropic) and $q^2$-dependent cross sections and compared them with the results obtained for the case of interactions with nucleons. They also calculated the evaporation mass for interactions with electrons and found it to be below the $GeV$ range, which would open a new mass window for searching for this type of scenarios.

## 7.2 Asteroseismic constraints on Asymmetric Dark Matter

To search for Dark matter, a complementary way is through asteroseismology. To understand this, in [17], they analysed the effects of Weakly Interactive Massive Particles (WIMPs)

and ADM in three stars [the Sun, KIC 7871531 ($0.85\,M_\odot$, 9.41 Gyr, A), and KIC 8379927 ($1.12\,M_\odot$, 1.82 Gyr, B)] using the core-sensitive asteroseismic ratio $r_{02}$. They attempted to constrain the effective spin-dependent DM-proton coupling for masses of a few GeV by comparing observational data with results of stellar models including DM energy transport.

They observed that the asteroseismic analysis disfavors the low mass, high cross section region of the ADM parameter space explored. Accumulation of WIMPs is considerably weaker, hence only the more massive star B is significantly affected.

## 7.3 New axion and hidden photon constraints from a solar data global fit

Helioseismology and solar neutrino observations can be used to obtain upper limits to the properties of non standard weakly interacting particles. In this work [18], they studied the case of models including axions and axion-like particles and the case of low mass hidden photons. In the analysis, they included the theoretical and observational errors and accounted for tensions between input parameters of solar models and have let the composition free to avoid the effect of solar abundance problem on the final result. The models were computed using GARSTEC code.

For axions they obtained an upper limit at $3\sigma$ for the axion-photon coupling constant of $g_{a\gamma} = 4.1 \cdot 10^{-10}$ GeV. For hidden photons the most restrictive upper limit available across a wide range of masses for the product of the kinetic mixing and mass of $\chi m < 1.8 \cdot 10^{-12}$ eV at $3\sigma$ was obtained. Both the constraints are better than the direct detection constraint of XENON10. They also checked that including hidden photons in solar models with AGSS09 composition degrades the agreement between models and helioseismology, and thus does not help in mitigating the solar abundance problem.

## 7.4 Weighing the Solar Axion

Axions and axion-like particles are low-mass pseudo-scalars that are expected to couple extremely weakly to standard model fields. They can convert into x-rays inside a long transverse magnetic field and can be observed through helioscopes via inverse Primakoff conversion in strong laboratory magnets pointed at the Sun. For masses greater than around 0.02 eV, the spectral oscillations present in the axion conversion signal are highly dependent on the axion mass and can be used to determine the axion mass to within percent-level accuracies. In the paper [19], they outlined the calculation of an axion signal inside IAXO and described the axion mass dependence. They demonstrated how well IAXO can distinguish the massive axion from a massless axion, and the accuracy to which the axion mass can be measured. They also showed that $> 3\sigma$ sensitivity to the axion mass is possible for axion masses down to $\sim 1 - 5 \times 10^{-3}$ eV.

## 7.5 Constraining dark photon properties with Asteroseismology

Dark photons can be produced in the stellar interiors at a rate that depends on both, the dark photon mass and its coupling to Standard Model particles (the kinetic mixing parameter $\chi$). In the work [20], they explored the changes in the internal structure of Red Giant Branch ( RGB) stars due to the an additional energy loss from dark photon emission from their degenerate cores. They have constrained the parameter space of dark photons using asteroseismic observables with a focus on the changes in the large frequency separation and the photometric properties of the RGB.

It was found that, at the RGB bump, the dark photons modify the internal structure and the depth of the convective borders, as well as produce an increase of density and asteroseismology is able to detect such variations in the structure, allowing us to predict an upper limit of 900 eV and $5 \times 10^{-15}$ for the mass and kinetic mixing of the dark photons, respectively. Also, dark photons increase the luminosity of the RGB tip (which corresponds to a local maximum in HR diagram by the He-flash) and can put additional constraints over the current observational uncertainties.

## 7.6 Helioseismic constraint on a cosmic-time variation of G

The gravitational constant G is not really a constant but evolves over cosmic time. Helioseismology can provide independent constraints on its evolution because the stellar luminosity $L$ varies as $\sim G^7$. In the work [21], they make use of the best possible estimate of 8640 days of low-$l$ BiSON data, corrected for the solar cycle variation for the new estimation of $G'/G_{\rm today}$. They built the solar model using GARSTEC code with the time evolution of the gravitational constant as a power-law. They used the frequency separation ratios $r_{l,l+2}(n)$ as the seismic diagnostics and by means of a Bayesian analysis both $G'/G_{\rm today}$ as well as $S_{pp}(0)$ (proton-proton (pp) fusion cross-section), have been estimated from the data and concluded that $G'/G_{\rm today} = (1.25 \pm 0.30) \times 10^{-13}$ yr$^{-1}$, a $4\sigma$ effect.

# Chapter 8

# Probing Dark Matter through Asteroseismology

## 8.1 Asteroseismology of Red Clump Stars as a Probe of the Dark Matter Content of the Galaxy Central Region

Red clump stars are core helium-burning stars located in the red end of the horizontal branch. These stars, in some cases with $L \simeq 10^2 L_{\odot}$, can be observed throughout the galaxy and thus can give us insight into the DM conditions found in situ. In this work [22], they considered thermally produced DM particles in the mass range 4–10 GeV with different values of DM density and spin-independent annihilation and scattering cross-sections that are close to the observational upper limits from direct detection experiments. To model the effects of DM in stars, they used MESA stellar evolution code with solar-like metallicity and initial helium mass fraction.

The results showed that the evacuation of energy via DM interactions with baryons can cease convection in the central region of the star, which will have a measurable impact on the asteroseismology of the star and can be observed. The impact will be more pronounced for lower DM mass and higher density. Considering that the DM density within a galaxy can widely vary from the periphery to the galactic center, the observation of a correspondence between the effects on period of oscillations and the distance to the galactic center would provide strong support for the large concentration of DM in the central region of the Milky Way.

## 8.2 Probing the Dark Matter-Electron Interactions via Hydrogen-Atmosphere Pulsating White Dwarfs

The hydrogen-atmosphere pulsating white dwarfs (DAVs) are a type of pulsating WD with hydrogen- dominated atmospheres and an electron-degenerate core. Precise asteroseismology on DAVs can reveal their interior structures and determine the rates of the period variations

and reveal the evolutionary cooling rates of DAVs which can be described by the Standard Cooling Model (SCM). In the work [23], they considered the DAVs in the central region of globular clusters (local DM-dense environments) and focussed on the DM-electron interactions. So in this case the DM particles, which are captured by multiple scattering with the DAVs' constituents mainly electrons, would annihilate by pairs and provide extra energy source to the stars. Thus the natural cooling process would be slowed down and could be detected by measuring the secular rates of the period variations.

The differences between the secular rates predicted by the precise asteroseismology and the secular rates obtained from observation can be used to constrain the DM-electron interactions. Combining with indirect DM detection results, this could give us a cross check on the existence of such leptonphilic DM particles to some extent.

# Bibliography


[1] S. Basu and H. Antia, "Helioseismology and solar abundances," *Physics Reports*, vol. 457, no. 5-6, pp. 217–283, mar 2008. [Online]. Available: https://doi.org/10.1016%2Fj.physrep.2007.12.002

[2] B. W. Carroll and D. A. Ostlie, *An Introduction to Modern Astrophysics*. Cambridge University Press, sep 2017. [Online]. Available: https://doi.org/10.1017%2F9781108380980

[3] M. Bergemann and A. Serenelli, "Solar abundance problem," in *Determination of Atmospheric Parameters of B-, A-, F- and G-Type Stars*. Springer International Publishing, 2014, pp. 245–258. [Online]. Available: https://doi.org/10.1007%2F978-3-319-06956-2_21

[4] S. Basu, "Global seismology of the sun," *Living Reviews in Solar Physics*, vol. 13, no. 1, aug 2016. [Online]. Available: https://doi.org/10.1007%2Fs41116-016-0003-4

[5] N. Grevesse and A. Sauval, *Space Science Reviews*, vol. 85, no. 1/2, pp. 161–174, 1998. [Online]. Available: https://doi.org/10.1023%2Fa%3A1005161325181

[6] M. Asplund, N. Grevesse, A. J. Sauval, and P. Scott, "The chemical composition of the sun," *Annual Review of Astronomy and Astrophysics*, vol. 47, no. 1, pp. 481–522, sep 2009. [Online]. Available: https://doi.org/10.1146%2Fannurev.astro.46.060407.145222

[7] J. Christensen-Dalsgaard, M. P. D. Mauro, G. Houdek, and F. Pijpers, "On the opacity change required to compensate for the revised solar composition," *Astronomy & Astrophysics*, vol. 494, no. 1, pp. 205–208, dec 2008. [Online]. Available: https://doi.org/10.1051%2F0004-6361%3A200810170

[8] S. Vagnozzi, K. Freese, and T. H. Zurbuchen, "Solar models in light of new high metallicity measurements from solar wind data," *The Astrophysical Journal*, vol. 839, no. 1, p. 55, apr 2017. [Online]. Available: https://doi.org/10.3847%2F1538-4357%2Faa6931

[9] D. G. Cerdeño, J. H. Davis, M. Fairbairn, and A. C. Vincent, "CNO neutrino grand prix: the race to solve the solar metallicity problem," *Journal of Cosmology and Astroparticle Physics*, vol. 2018, no. 04, pp. 037–037, apr 2018. [Online]. Available: https://doi.org/10.1088%2F1475-7516%2F2018%2F04%2F037

[10] M. Agostini *et al.*, "Sensitivity to neutrinos from the solar CNO cycle in Borexino," *Eur. Phys. J. C*, vol. 80, no. 11, p. 1091, 5 2020.

[11] D. O. Gough, "Anticipating the sun's heavy-element abundance," *Monthly Notices of the Royal Astronomical Society: Letters*, vol. 485, no. 1, pp. L114–L115, mar 2019. [Online]. Available: https://doi.org/10.1093%2Fmnrasl%2Fslz044

[12] N. Song, M. C. Gonzalez-Garcia, F. L. Villante, N. Vinyoles, and A. Serenelli, "Helioseismic and neutrino data-driven reconstruction of solar properties," *Monthly Notices of the Royal Astronomical Society*, vol. 477, no. 1, pp. 1397–1413, mar 2018. [Online]. Available: https://doi.org/10.1093%2Fmnras%2Fsty600

[13] A. Sokolov, "Generic energy transport solutions to the solar abundance problem—a hint of new physics," *Journal of Cosmology and Astroparticle Physics*, vol. 2020, no. 03, pp. 013–013, mar 2020. [Online]. Available: https://doi.org/10.1088%2F1475-7516%2F2020%2F03%2F013

[14] A. C. Vincent, A. Serenelli, and P. Scott, "Generalised form factor dark matter in the sun," *Journal of Cosmology and Astroparticle Physics*, vol. 2015, no. 08, pp. 040–040, aug 2015. [Online]. Available: https://doi.org/10.1088%2F1475-7516%2F2015%2F08%2F040

[15] A. C. Vincent, P. Scott, and A. Serenelli, "Possible indication of momentum-dependent asymmetric dark matter in the sun," *Physical Review Letters*, vol. 114, no. 8, feb 2015. [Online]. Available: https://doi.org/10.1103%2Fphysrevlett.114.081302

[16] R. Garani and S. Palomares-Ruiz, "Dark matter in the sun: scattering off electrons vs nucleons," *Journal of Cosmology and Astroparticle Physics*, vol. 2017, no. 05, pp. 007–007, may 2017. [Online]. Available: https://doi.org/10.1088%2F1475-7516%2F2017%2F05%2F007

[17] A. Martins, I. Lopes, and J. Casanellas, "Asteroseismic constraints on asymmetric dark matter: Light particles with an effective spin-dependent coupling," *Physical Review D*, vol. 95, no. 2, jan 2017. [Online]. Available: https://doi.org/10.1103%2Fphysrevd.95.023507

[18] N. Vinyoles, A. Serenelli, F. Villante, S. Basu, J. Redondo, and J. Isern, "New axion and hidden photon constraints from a solar data global fit," *Journal of Cosmology and Astroparticle Physics*, vol. 2015, no. 10, pp. 015–015, oct 2015. [Online]. Available: https://doi.org/10.1088%2F1475-7516%2F2015%2F10%2F015

[19] T. Dafni, C. A. O'Hare, B. Lakić, J. Galán, F. J. Iguaz, I. G. Irastorza, K. Jakovčić, G. Luzón, J. Redondo, and E. R. Chóliz, "Weighing the solar axion," *Physical Review D*, vol. 99, no. 3, feb 2019. [Online]. Available: https://doi.org/10.1103%2Fphysrevd.99.035037

[20] A. Ayala, I. Lopes, A. G. Hernández, J. C. Suárez, and Í. M. Elorza, "Constraining dark photon properties with asteroseismology," *Monthly Notices of the Royal*

*Astronomical Society*, vol. 491, no. 1, pp. 409–416, oct 2019. [Online]. Available: https://doi.org/10.1093%2Fmnras%2Fstz3002

[21] A. Bonanno and H.-E. Fröhlich, "A new helioseismic constraint on a cosmic-time variation of G," *Astrophys. J. Lett.*, vol. 893, no. 2, p. L35, 2020.

[22] J. Lopes, I. Lopes, and J. Silk, "Asteroseismology of red clump stars as a probe of the dark matter content of the galaxy central region," *The Astrophysical Journal*, vol. 880, no. 2, p. L25, jul 2019. [Online]. Available: https://doi.org/10.3847%2F2041-8213%2Fab2fdd

[23] J.-S. Niu, T. Li, W. Zong, H.-F. Xue, and Y. Wang, "Probing the dark matter-electron interactions via hydrogen-atmosphere pulsating white dwarfs," *Physical Review D*, vol. 98, no. 10, nov 2018. [Online]. Available: https://doi.org/10.1103%2Fphysrevd.98.103023

[24] and and, "Detailed opacity calculations for astrophysical applications," *Atoms*, vol. 5, no. 4, p. 22, may 2017. [Online]. Available: https://doi.org/10.3390%2Fatoms5020022